NIH Public Access
Author Manuscript
Magn Reson Insights. Author manuscript; available in PMC 2012 May 23.

Published in final edited form as:
Magn Reson Insights. 2012 March 29; 5: 1–6. doi:10.4137/MRI.S9352.

Improvements in a Mouse Model of Alzheimer's Disease Through SOD2 Overexpression are Due to Functional and Not Structural Alterations

Brittany R. Bitner[1], **Carlos J. Perez-Torres**[1], **Lingyun Hu**[2,3], **Taeko Inoue**[2], and **Robia G. Pautler**[1,2]

[1]Interdepartment program in Translation Biology and Molecular Medicine, Baylor College of Medicine, One Baylor Plaza, Houston TX 77030

[2]Department of Molecular Physiology and Biophysics, Baylor College of Medicine, One Baylor Plaza, Houston TX 77030

[3]Novartis Institutes for BioMedical Research, Inc., Cambridge, MA

Abstract

Oxidative stress and mitochondrial dysfunction have been implicated in the pathogenesis of Alzheimer's disease. We and others have shown that over expression of the mitochondrial antioxidant superoxide dismutase 2 (SOD-2) can improve many of the pathologies in the Tg2576 mouse model of Alzheimer's disease that harbors the Swedish mutation in the amyloid precursor protein. However, it is not clear if these improvements are due to functional improvements or structural/anatomical changes. To answer this question, we used diffusion tensor imaging (DTI) to assess the structural integrity of white matter tracts in the control mice, Tg2576 mouse and Tg2576 mice over expressing SOD-2. We observed minimal differences in diffusion parameters with SOD-2 over expression in this model indicating that the improvements we previously reported are due to functional changes and not any alterations to the white matter tractography.

Keywords

superoxide dismutase 2; Alzheimer's Disease; diffusion tensor imaging; mouse; Tg2576

© the author(s), publisher and licensee Libertas Academica Ltd.

Corresponding author: rpautler@bcm.edu.

This is an open access article. Unrestricted non-commercial use is permitted provided the original work is properly cited.

Author Contributions

Conceived and designed the experiments: RGP, BRB, LH. Analysed the data: BRB, CJP, LH. Wrote the first draft of the manuscript: BRB. Contributed to the writing of the manuscript: CJP, TI. Agree with manuscript results and conclusions: RGP, BRB, CJP, LH, TI. Jointly developed the structure and arguments for the paper: RGP, BRB. Made critical revisions and approved final version: BRB. All authors reviewed and approved of the final manuscript.

Disclosures and Ethics

As a requirement of publication author(s) have provided to the publisher signed confirmation of compliance with legal and ethical obligations including but not limited to the following: authorship and contributorship, conflicts of interest, privacy and confidentiality and (where applicable) protection of human and animal research subjects. The authors have read and confirmed their agreement with the ICMJE authorship and conflict of interest criteria. The authors have also confirmed that this article is unique and not under consideration or published in any other publication, and that they have permission from rights holders to reproduce any copyrighted material. Any disclosures are made in this section. The external blind peer reviewers report no conflicts of interest.

NIH-PA Author Manuscript
NIH-PA Author Manuscript
NIH-PA Author Manuscript

NIH-PA Author Manuscript

NIH-PA Author Manuscript

NIH-PA Author Manuscript

Introduction

Alzheimer's disease (AD) is an age-related neurodegenerative disease that is currently the 6th leading cause of death among American adults.[1] AD involves progressive memory loss and cognitive decline.[2] The hallmark histological findings of AD are extracellular deposits of amyloid-beta (Aβ) known as plaques and intracellular aggregates of hyperphosphorylated tau known as neurofibrillary tangles.[3] More recently, grey and white matter changes have been detected in both AD patients and some animal models of AD with diffusion tensor imaging.[4–6] Although Aβ's neurotoxic potential is well established,[7] its exact role in the molecular mechanisms leading to the development of AD is unclear.

Oxidative stress has been strongly implicated in neurodegenerative diseases such as AD.[8] Aβ can induce oxidation reactions,[9,10] and in turn, a pro-oxidant state can increase the levels of Aβ.[11] Mitochondria, as the powerhouses of the cell, produce significant amounts of reactive oxygen species (ROS) such as superoxide anion.[12,13] Moreover, mitochondrial abnormalities and oxidative damage have been reported to be involved in the disease processes of AD.[14,15]

In the mitochondria, superoxide dismutase-2 (SOD-2) is a scavenger of superoxide anions.[16] AD mouse models with reduced expression of SOD-2 have accelerated cognitive dysfunction and increased levels of Aβ in the brain.[17,18] We and others have also shown that over expression of SOD-2 in an AD mouse model prevented memory impairments, reduced Aβ plaques, improved axonal transport and cerebral blood flow, and rescued hippocampal synaptic plasticity.[19–21] The question remains though, whether these improvements are due to functional improvements or structural components or a combination of both. It is not known if the SOD-2 over expression that recovers axonal transport and synaptic plasticity is also associated with white matter changes. Using diffusion tensor imaging (DTI) to measured white matter integrity parameters (axonal diffusivity, fractional anisotropy, and trace), we investigated whether SOD-2 over expression can alter white matter integrity in the Tg2576 mouse model of amyloidosis.

Materials and Methods

Animal protocol

All experimental procedures were performed in accordance with the Institutional Animal Care and Use Committee of Baylor College of Medicine. The Tg2576 transgenic mice carrying the Swedish mutation human amyloid precursor protein (Tg2576), the mitochondrial superoxide dismutase over expressing (SOD2) transgenic mice, and the double transgenic SOD2/Tg2576 transgenic (SOD2/Tg2576) mice have already been described.[19,22,23] 15–21 month old SOD2/Tg2576, SOD2, Tg2576, and wildtype (WT) littermate mice were deeply anesthetized using a ketamine and zylazine cocktail. Fixed brains for MRI were prepared as described in Tyszka et al.[24] Briefly, the mice were transcardially perfused with heparinized phosphate buffered saline (PBS) followed by fixation with 4% paraformaldehyde (PFA). Post perfusion, the head was removed. The skin, muscle, ears, nose tip, and lower jaw were removed to expose the skull. The head was fixed overnight in 4% PFA at 4 °C. The head was then transferred to 40 mLs of 0.01% sodium azide in PBS and rocked for 7 days at 4 °C. The head was transferred to a solution of 5 mM gadopentate dimeglumine (Bayer HealthCare Pharmaceuticals Inc., Wayne, NJ) and 0.01% sodium azide in PBS and rocked for 21–24 days at 4 °C. Incubation with gadopentate dimeglumine improved the signal-to-noise ratio. Prior to imaging, the head was equilibrated to room temperature for 6–8 hours.

NIH-PA Author Manuscript

NIH-PA Author Manuscript

NIH-PA Author Manuscript

Magnetic resonance protocol

All scans were acquired on a 9.4 T Bruker Avance Biospec Spectrometer, 21-cm bore horizontal scanner with 35 mm volume resonator (Bruker BioSpin, Billerica, MA) with Paravision 4.0 software (Bruker Biospin, Billerica, MA). An initial pilot scan was run to position the DTI scan. The 3D DTI scan parameters are as follows: Spin echo, b-value = 0 and 1000s/mm^2, 20 diffusion directions with one non-diffusion weighted image, TR = 500 ms, TE = 14.8 ms, FOV = 1.5 × 1.0 × 2.0 cm, matrix = 164 × 96 × 96, NEX = 1, δ = 3 ms, Δ = 7 ms. The acquisition time = ~15 hrs.

Image processing

The MRI images were first processed on Amira (Visage Imaging, Inc., San Diego, CA) to remove skull and extraneous tissue from the images in preparation for alignment. The non-diffusion weighted image for each genotype was then aligned to one brain within each group using BUILD.[25–27] The groups were aligned together. DTI studio[28] was used to calculate the trace, the primary eigenvalue (λ_{II}, often referred to as axial diffusivity), and fractional anisotrophy (FA) from six brain regions of interest (ROIs, Fig. 1). The ROI were defined for the corpus callosum (CC), cingulum (cg), external capsule (EC), dorsal hippocampal commissure (DHC), ventral hippocampal commissure (VHC), anterior commisure (AC). The 3D ROI were manually drawn on one brain and then the regions were applied to the native diffusion weighted images of the other brains using the alignment information.

Statistics

Brain ROIs were analyzed separately. Values for diffusion were calculated as the mean of each measure across all of the voxels in a particular 3D ROI for each brain. One-way ANOVA was used to determine if there was a significant difference in diffusion parameters between WT, SOD2, Tg2576, and SOD2/Tg2576 mice. *P*-values for diffusion data were adjusted for the multiple comparisions of trace, λ_{II}, and FA by using a *P*-value <0.0167 as significant (0.05/3).

Results

Age and ROI

There was no significant difference in the mean age of mice from each group ($P = 0.9345$). The sizes of all of the ROIs were not significantly different between groups except the VHC ($P = 0.0114$) where the SOD2 animals had a slightly larger VHC compared to Tg2576 (Bonferroni post test $P < 0.05$, Fig. 2).

Diffusion parameters

To perform quantitative comparison of the groups, the rotational invariant diffusion tensor parameters of fractional anisotropy (FA), primary eigenvalue (axial diffusivity), and the trace (total diffusivity) were calculated. There was no significant difference between the four groups in trace or axial diffusivity for any of the ROIs (Table 1) after a one-way ANOVA. The FA in the anterior commissure (AC) was significantly different ($P = 0.0109$; Fig. 3) and a Bonferroni post-test showed that SOD2/Tg2576 mice had higher FA than both Tg2576 and SOD2 (Bonferroni post test, $P < 0.05$ and $P < 0.01$, respectively).

Discussion

In the Tg2576 mouse model of amyloidosis, we and others have shown that SOD-2 over expression can restore cerebral blood flow, reduce plaque load, decrease oxygen radical levels, improve behavioral outcomes, and recover axonal transport and synaptic

NIH-PA Author Manuscript

NIH-PA Author Manuscript

NIH-PA Author Manuscript

plasticity.[19–21] From our data presented here, the improvements from SOD-2 over expression appear to be functional rather than structural or anatomical changes in fixed brains from Tg2576 mice since the majority of diffusion parameters were not significantly different between groups. At the age point tested, approximately 18 months, SOD2/Tg2576 mice only showed a small increase in FA in the anterior commissure compared to SOD2 mice with a non-significant trend toward higher FA compared to Tg2576 mice. There was a difference in VHC size. The reason for the differences in size of the VHC ROI is not clear. As has already been shown in this model, the Tg2576 mouse, although a model of human amyloid over expression, it does not exhibit the significant neuro degeneration that is seen in human Alzheimer's patients.[22,29]

Other groups have reported minor differences in diffusion parameters in the Tg2576 mouse model and another mouse model of brain amyloidosis (the PDAPP mouse); however these changes were not progressive and tended to be small.[5,6] In addition, these studies were performed with 6 diffusion directions for calculating diffusion parameters; however, a Monte Carlo simulation study found that for robust estimations of anisotrophy at least 20 diffusion directions are necessary.[30] A more recent study by Harm et al using fixed brains from Tg2576 mice with 20 diffusion directions found small reductions in relative anisotrophy (2%–6%) in the CC and VHC but these changes were not progressive with age.[31] They also found no significant differences in other diffusion parameters in the AC, posterior commissure, fornix, and dorsal fornix.[31]

Our study was restricted to using perfusion fixed brains because of the time restraint imposed by the imaging time which was approximately 15 hours. It is not clear if there are differences between in vivo and ex vivo diffusion indices. Sun et al. reported preservation of relative anisotrophy with fixation since there was a proportional decrease in the diffusion coefficients in all directions equally.[32,33] Another comparison of live versus fixed tissue anisotropy has found differences; however, the validity of the finding is questionable since the number of diffusion directions between the live versus fixed tissue was not the same (6 versus 20).[6,31]

In conclusion, little to no diffusion changes were seen in the white matter tracts of the brains from WT, SOD2, Tg2576, and SOD2/Tg2576 mice. Only the anterior commissure in SOD2/Tg2576 had a small but significant increase in FA compared to SOD2 mice. This is consistent with only minor changes being detected in this same model with 20 diffusion direction DTI.[31] SOD-2 over expression in the Tg2576 mouse model of amyloidosis has been shown to improve many of the pathological consequences and behavioral sequelae of amyloid over expression; however, the magnitude of these improvements cannot be explained by the minor differences in diffusion parameters reported here. This suggests that SOD-2 over expression and reduction of ROS may be more of a functional recovery instead of a structural or anatomical improvement.

Acknowledgments

The authors thank Professor Susan G. Hilsenbeck for assistance with statistical analysis. We also acknowledge NIH/NIA R01 AG029977. We also thank Dr. Mark Henkelman, John Sled and Jason Lerch (Mouse Imaging Centre, Hospital for Sick Children, Toronto, Canada) for providing the BUILD software used for some of the image registration.

Funding

This work was supported by the following funding sources: NIH/NIA R01AG029977 (PI: Dr. Robia Pautler) and NIH/NIDDK P30DK079638 MRI Core (PI: Dr. Larry Chan, Core Director, Dr. Robia Pautler).

NIH-PA Author Manuscript

NIH-PA Author Manuscript

NIH-PA Author Manuscript

References

1. Xu, J.; Kochanek, K.; Murphy, S.; Tejada-Vera, B. Deaths: Final Data for 2007. Hyattville, MD: National Center for Health Statistics; 2010. Available at: http://www.ncbi.nlm.nih.gov/pubmed/
2. Lindeboom J, Weinstein H. Neuropsychology of cognitive ageing, minimal cognitive impairment, Alzheimer's disease, and vascular cognitive impairment. Eur J Pharmacol. 2004; 490(1–3):83–6. [PubMed: 15094075]
3. Götz J, Schild A, Hoerndli F, Pennanen L. Amyloid-induced neurofibrillary tangle formation in Alzheimer's disease: insight from transgenic mouse and tissue-culture models. Int J Dev Neurosci. 2004; 22(7):453–65. [PubMed: 15465275]
4. Bozzali M, Falini A, Franceschi M, et al. White matter damage in Alzheimer's disease assessed in vivo using diffusion tensor magnetic resonance imaging. J Neurol Neurosurg Psychiatr. 2002; 72(6):742–6. [PubMed: 12023417]
5. Song S-K, Kim JH, Lin S-J, Brendza RP, Holtzman DM. Diffusion tensor imaging detects age-dependent white matter changes in a transgenic mouse model with amyloid deposition. Neurobiol Dis. 2004; 15(3):640–7. [PubMed: 15056472]
6. Sun S-W, Song S-K, Harms MP, et al. Detection of age-dependent brain injury in a mouse model of brain amyloidosis associated with Alzheimer's disease using magnetic resonance diffusion tensor imaging. Exp Neurol. 2005; 191(1):77–85. [PubMed: 15589514]
7. Yankner BA, Dawes LR, Fisher S, et al. Neurotoxicity of a fragment of the amyloid precursor associated with Alzheimer's disease. Science. 1989; 245(4916):417–20. [PubMed: 2474201]
8. Lin MT, Beal MF. Mitochondrial dysfunction and oxidative stress in neurodegenerative diseases. Nature. 2006; 443(7113):787–95. [PubMed: 17051205]
9. Butterfield DA, Griffin S, Munch G, Pasinetti GM. Amyloid beta-peptide and amyloid pathology are central to the oxidative stress and inflammatory cascades under which Alzheimer's disease brain exists. J Alzheimers Dis. 2002; 4(3):193–201. [PubMed: 12226538]
10. Behl C, Davis JB, Lesley R, Schubert D. Hydrogen peroxide mediates amyloid beta protein toxicity. Cell. 1994; 77(6):817–27. [PubMed: 8004671]
11. Tamagno E, Parola M, Bardini P, et al. Beta-site APP cleaving enzyme up-regulation induced by 4-hydroxynonenal is mediated by stress-activated protein kinases pathways. J Neurochem. 2005; 92(3):628–36. [PubMed: 15659232]
12. Balaban RS, Nemoto S, Finkel T. Mitochondria, oxidants, and aging. Cell. 2005; 120(4):483–95. [PubMed: 15734681]
13. Murphy MP. How mitochondria produce reactive oxygen species. Biochem J. 2009; 417(1):1–13. [PubMed: 19061483]
14. Zhu X, Lee H-G, Casadesus G, et al. Oxidative imbalance in Alzheimer's disease. Mol Neurobiol. 2005; 31(1–3):205–17. [PubMed: 15953822]
15. Reddy PH, Beal MF. Are mitochondria critical in the pathogenesis of Alzheimer's disease? Brain Res Brain Res Rev. 2005; 49(3):618–32. [PubMed: 16269322]
16. Weisiger RA, Fridovich I. Superoxide dismutase. Organelle specificity. J Biol Chem. 1973; 248(10):3582–92. [PubMed: 4702877]
17. Li F, Calingasan NY, Yu F, et al. Increased plaque burden in brains of APP mutant MnSOD heterozygous knockout mice. J Neurochem. 2004; 89(5):1308–12. [PubMed: 15147524]
18. Esposito L, Raber J, Kekonius L, et al. Reduction in mitochondrial super-oxide dismutase modulates Alzheimer's disease-like pathology and accelerates the onset of behavioral changes in human amyloid precursor protein transgenic mice. J Neurosci. 2006; 26(19):5167–79. [PubMed: 16687508]
19. Massaad CA, Washington TM, Pautler RG, Klann E. Overexpression of SOD-2 reduces hippocampal superoxide and prevents memory deficits in a mouse model of Alzheimer's disease. Proc Natl Acad Sci U S A. 2009; 106(32):13576–81. [PubMed: 19666610]
20. Ma T, Hoeffer CA, Wong H, et al. Amyloid β-induced impairments in hippocampal synaptic plasticity are rescued by decreasing mitochondrial superoxide. J Neurosci. 2011; 31(15):5589–95. [PubMed: 21490199]

NIH-PA Author Manuscript

NIH-PA Author Manuscript

NIH-PA Author Manuscript

21. Massaad CA, Amin SK, Hu L, et al. Mitochondrial superoxide contributes to blood flow and axonal transport deficits in the Tg2576 mouse model of Alzheimer's disease. PLoS ONE. 2010; 5(5):e10561. [PubMed: 20479943]
22. Hsiao K, Chapman P, Nilsen S, et al. Correlative memory deficits, Abeta elevation, and amyloid plaques in transgenic mice. Science. 1996; 274(5284):99–102. [PubMed: 8810256]
23. Ho YS, Vincent R, Dey MS, Slot JW, Crapo JD. Transgenic models for the study of lung antioxidant defense: enhanced manganese-containing superoxide dismutase activity gives partial protection to B6C3 hybrid mice exposed to hyperoxia. Am J Respir Cell Mol Biol. 1998; 18(4): 538–47. [PubMed: 9533942]
24. Tyszka JM, Readhead C, Bearer EL, Pautler RG, Jacobs RE. Statistical diffusion tensor histology reveals regional dysmyelination effects in the shiverer mouse mutant. Neuroimage. 2006; 29(4): 1058–65. [PubMed: 16213163]
25. Lerch JP, Sled JG, Henkelman RM. MRI phenotyping of genetically altered mice. Methods Mol Biol. 2011; 711:349–61. [PubMed: 21279611]
26. Collins DL, Neelin P, Peters TM, Evans AC. Automatic 3D intersubject registration of MR volumetric data in standardized Talairach space. J Comput Assist Tomogr. 1994; 18(2):192–205. [PubMed: 8126267]
27. Collins DL, Holmes CJ, Peters TM, Evans AC. Automatic 3-D model-based neuroanatomical segmentation. Human Brain Mapping. 1995; 3(3):190–208.
28. Jiang H, van Zijl PCM, Kim J, Pearlson GD, Mori S. DtiStudio: resource program for diffusion tensor computation and fiber bundle tracking. Comput Methods Programs Biomed. 2006; 81(2): 106–16. [PubMed: 16413083]
29. Kawarabayashi T, Younkin LH, Saido TC, et al. Age-dependent changes in brain, CSF, and plasma amyloid (beta) protein in the Tg2576 transgenic mouse model of Alzheimer's disease. J Neurosci. 2001; 21(2):372–81. [PubMed: 11160418]
30. Jones DK. The effect of gradient sampling schemes on measures derived from diffusion tensor MRI: a Monte Carlo study. Magn Reson Med. 2004; 51(4):807–15. [PubMed: 15065255]
31. Harms MP, Kotyk JJ, Merchant KM. Evaluation of white matter integrity in ex vivo brains of amyloid plaque-bearing APPsw transgenic mice using magnetic resonance diffusion tensor imaging. Exp Neurol. 2006; 199(2):408–15. [PubMed: 16483571]
32. Sun S-W, Neil JJ, Song S-K. Relative indices of water diffusion anisotropy are equivalent in live and formalin-fixed mouse brains. Magn Reson Med. 2003; 50(4):743–8. [PubMed: 14523960]
33. Sun S-W, Neil JJ, Liang H-F, et al. Formalin fixation alters water diffusion coefficient magnitude but not anisotropy in infarcted brain. Magn Reson Med. 2005; 53(6):1447–51. [PubMed: 15906292]

NIH-PA Author Manuscript
NIH-PA Author Manuscript
NIH-PA Author Manuscript

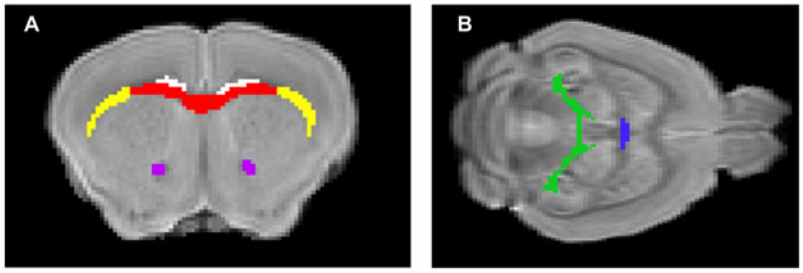

Figure 1.

Regions of interest (ROI) for diffusion measurements. Non-diffusion weighted images of a mouse brain in (**A**). Coronoal view of brain with ROI for corpus callosum (red), external capsule (yellow), cingulum (white), and anterior commissure (purple) or (**B**). Horizontal view with ROI for dorsal hippocampal commissure (green) and ventral hippocampal commissure (blue).

NIH-PA Author Manuscript

NIH-PA Author Manuscript

NIH-PA Author Manuscript

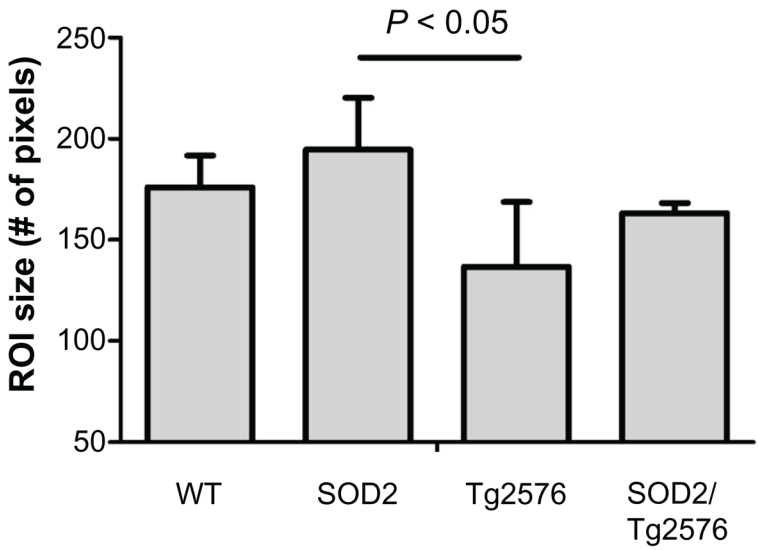

Figure 2.
The size of the ROI for the ventral hippocampal commissure is significantly different between groups.
Notes: Bonferroni post test reveals that the SOD2 group has a significantly larger VHC ROI than Tg2576 group ($P < 0.05$). Values are mean ± standard deviation.

NIH-PA Author Manuscript

NIH-PA Author Manuscript

NIH-PA Author Manuscript

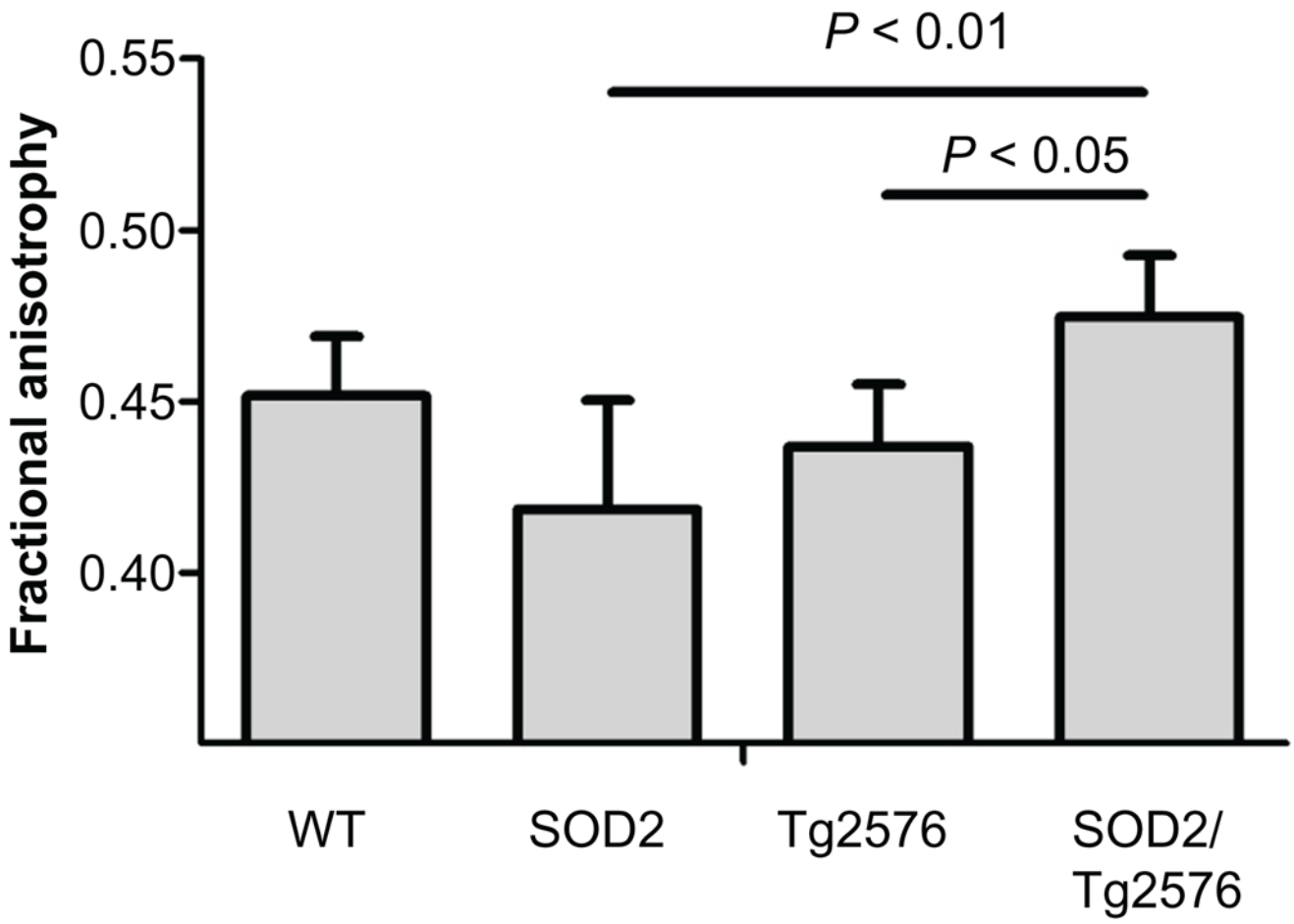

Figure 3.
Fractional anisotrophy is increased in SOD2/Tg2576 mice compared to Tg2576 and SOD2 mice.
Note: Values are mean ± standard deviation.

NIH-PA Author Manuscript

NIH-PA Author Manuscript

NIH-PA Author Manuscript

Table 1

Diffusion measures.

	WT (n = 4)	SOD-2 (n = 4)	Tg2576 (n = 5)	SOD2/Tg2576 (n = 5)
CC				
FA	0.496 ± 0.020	0.503 ± 0.056	0.471 ± 0.053	0.546 ± 0.028
λ_{ll}	0.358 ± 0.072	0.429 ± 0.025	0.404 ± 0.046	0.422 ± 0.024
Trace	0.800 ± 0.053	0.842 ± 0.064	0.814 ± 0.129	0.756 ± 0.057
cg				
FA	0.485 ± 0.015	0.494 ± 0.056	0.462 ± 0.045	0.507 ± 0.023
λ_{ll}	0.339 ± 0.084	0.411 ± 0.030	0.394 ± 0.037	0.421 ± 0.023
Trace	0.742 ± 0.042	0.793 ± 0.048	0.789 ± 0.092	0.777 ± 0.053
DHC				
FA	0.543 ± 0.018	0.520 ± 0.061	0.487 ± 0.020	0.530 ± 0.039
λ_{ll}	0.421 ± 0.120	0.503 ± 0.024	0.481 ± 0.028	0.490 ± 0.025
Trace	0.875 ± 0.048	0.934 ± 0.045	0.918 ± 0.062	0.880 ± 0.033
VHC				
FA	0.513 ± 0.043	0.488 ± 0.107	0.495 ± 0.072	0.517 ± 0.019
λ_{ll}	0.379 ± 0.059	0.436 ± 0.057	0.407 ± 0.068	0.425 ± 0.019
Trace	0.822 ± 0.116	0.869 ± 0.194	0.786 ± 0.152	0.825 ± 0.039
EC				
FA	0.370 ± 0.012	0.397 ± 0.057	0.377 ± 0.038	0.419 ± 0.026
λ_{ll}	0.401 ± 0.073	0.432 ± 0.030	0.423 ± 0.020	0.429 ± 0.018
Trace	0.948 ± 0.063	0.914 ± 0.053	0.911 ± 0.071	0.870 ± 0.040
AC				
FA	0.452 ± 0.017	0.411 ± 0.041	0.437 ± 0.018	0.475 ± 0.018
λ_{ll}	0.408 ± 0.105	0.461 ± 0.032	0.392 ± 0.049	0.451 ± 0.041
Trace	0.915 ± 0.064	0.955 ± 0.085	0.794 ± 0.099	0.833 ± 0.056

Notes: Values are mean ± SD. All $\lambda_{||}$ and trace values are 1×10^{-3} mm^2/s.